

# Association of Tumor Washout Rates and Accumulation of Technetium-99m-MIBI with Expression of P-Glycoprotein in Lung Cancer

Lale Kostakoglu, Pinar Kiratli, Şevket Ruacan, Mutlu Hayran, Salih Emri, Eser L. Ergün and Coşkun F. Bekdik  
Departments of Nuclear Medicine, Pathology and Cancer Epidemiology and Service of Pulmonary Diseases, Medical Faculty, Hacettepe University, Ankara, Turkey

In a prospective study, we correlated the washout rates of  $^{99m}\text{Tc}$ -sestamibi (MIBI) and the degree of MIBI accumulation with the expression of P-glycoprotein (Pgp) in tumor tissues in a total of 46 patients with lung cancer. **Methods:** All patients underwent early (30 min) and delayed (3 hr) MIBI imaging and bronchoscopic biopsy before initiation of chemo- or radiotherapy. The interval between biopsy and imaging varied between 2 and 10 days. All patients had radiologically detectable tumors. Immunohistochemical studies were performed on paraffin sections using a monoclonal antibody, JSB-1, developed against the internal epitope of Pgp. Normal tissue and tumor washout rates and tumor-to-background ratios were correlated with the level of Pgp expression. **Results:** There was an inverse correlation between tumor-to-background ratios and the density of Pgp ( $p = 0.001$ ), whereas there was no appreciable correlation between tumor washout rates of MIBI and the level of Pgp expression ( $p = 0.414$ ). **Conclusion:** The current data strongly suggest that, although the reduced ability for the tumors to accumulate MIBI correlates well with the increased levels of Pgp expression, tumor washout rates of MIBI do not correlate with the density of Pgp in tumor tissues. Our results also warrant additional research for correlating immunohistological and imaging findings with messenger RNA levels determined by polymerase chain reaction and flow cytometry.

**Key Words:** multidrug resistance; *MDR1* gene; P-glycoprotein; technetium-99m-sestamibi; washout

*J Nucl Med* 1998; 39:228-234

Determining the mechanisms of drug resistance is imperative to the development of rational therapeutic strategies. Because causes of chemotherapy failure are multifactorial, a major advance in the treatment of patients with neoplastic disease would be the identification of specific markers, predictive of drug resistance, expressed by tumors either at presentation or during therapy. One mechanism of resistance that has been well-characterized is that of multidrug resistance (MDR) (1). The most consistent alteration found in MDR cell lines is the increased expression of a high molecular weight cell surface glycoprotein, P-glycoprotein (Pgp), and, concomitantly, reduced ability to accumulate and retain drugs due to the energy-dependent Pgp efflux pump, which has a central role in the transport of drugs through the cell membrane (2,3). Despite extensive investigations completed in this field, the kinetics of drug transport in MDR cells still remain to be fully defined. Evidently, the drug influx and its intracellular binding, metabolism and efflux all contribute to the resulting reduced accumulation of each drug affected by the MDR phenotype. However, considering decrease in steady-state drug accumulation and efflux of the substrates as two separate parameters, the

extent of contribution of each parameter to the Pgp mechanism is still an ongoing laboratory curiosity (4).

Recent data have demonstrated that MIBI, as a lipophilic and cationic complex, is recognized as a transport substrate by the Pgp efflux pump. Not surprisingly, overexpression of Pgp in cell lines responsible for the altered permeability properties of resistant cells was found to transport MIBI outside the cell, rendering its intracellular accumulation lower than the expected range (5-7). Therefore, the information that could be derived from MIBI imaging might be used in the prediction of the course of cancer by identifying patients who will not respond to conventional chemotherapy and could guide the design of the most effective therapy protocols by allowing the inclusion of MDR modulators. However, the paucity of completed clinical studies could be held accountable for mitigating the clinical use of MIBI imaging in noninvasively determining the presence of Pgp overexpression.

Briefly, the need for extended clinical studies to contribute to the existing data have provided a basis for this study, which is an attempt to determine whether or not there is any association of the levels of Pgp expression with MIBI tumor washout rates and the magnitude of MIBI accumulation in tumor tissues in patients with lung cancer.

## MATERIALS AND METHODS

### Patient Population

A total of 46 patients (41 men, 5 women; age range 34-76 yr; mean age 58 yr) were included in the study. Twenty-six patients had squamous cell carcinoma, and 20 had small-cell lung cancer (SCLC). None had received previous chemo- or radiotherapy. All tumors were radiographically detected by CT or chest radiograph, and the presence of tumors was confirmed by histology. All patients had bronchoscopic biopsy either 3-5 days before (36 patients) or 5-10 days after (10 patients) MIBI imaging. All tumor specimens were evaluated for levels of Pgp expression by immunohistochemical analysis. Immunostaining was performed only on tumor specimens, and no normal lung tissue was obtained for immunohistochemistry.

### Imaging

A dual-head ADAC Genesys camera with a low-energy, high-resolution collimator was used for image acquisition. Images were obtained 20-30 min and 3-3.5 hr after the injection of 740 MBq  $^{99m}\text{Tc}$ -MIBI. Early and delayed spot images and early SPECT study of the chest were acquired in all patients. Both early and delayed SPECT and planar images were obtained in 23 patients (Table 1). SPECT was performed using a matrix size of  $64 \times 64 \times 646$  for 64 projections and an imaging time of 30 sec per projection. The tomographic images were reconstructed using a Butterworth filter with a cutoff frequency of 0.35 and an order of 6. Attenuation correction was applied to all frames.

Received Jan. 9, 1997; revision accepted Apr. 15, 1997.

For correspondence or reprints contact: Lale Kostakoglu, MD, New York Hospital-Cornell Medical Center, Division of Nuclear Medicine, 525 E. 68th St., Starr Bldg. 221, New York, NY 10021.

**TABLE 1**  
Comparison of Washout Rates on Planar and SPECT Images

Patient no.	SPECT		Planar		Pgp	Group
	Tumor %W-O/hr	Normal tissue % W-O/hr	Tumor %W-O/hr	Normal tissue %W-O/hr		
1	10	15	10	10.5	+++	3
2	12	12	9.0	10	++	3
3	12	15	9.0	9.0	++	3
4	6.0	4.0	7.0	6.0	++	3
5	15	18	16	14	++	3
6	13	14	13	13	+	2
7	15	14	16	16	+	2
8	16	11	14	12.5	f+	2
9	18	14	12	12	f+	2
10	21	18	17	11	f+	2
11	16 nec	9.5	14	8.0	f+	2
12	7.0	5.0	12	10	-	1
13	15	13	8.0	4.6	-	1
14	14	12	9.0	9.0	-	1
15	16	15	5.0	4.8	-	1
16	15	13	13	11	-	1
17	10	6.5	16	14	-	1
18	14	12	11	9.0	-	1
19	15 nec	10	13	11	-	1
20	15 nec	14	13	10	-	1
21	17 nec	14	13	12	-	1
22	12	9.0	13	14	-	1
23	16 nec	13	12	12	-	1

nec = necrotic tumor detected by radiographical modalities or histology.

The parameters investigated on MIBI images were tumor-to-background (tm/bkg) ratios and tumor and normal tissue percentage washout rates per hour (%W-O/hr). Tumor-to-background ratios were calculated by drawing a region of interest (ROI) over the tumor and contralateral site, using early SPECT study, on consecutive transverse sections including the entire tumor volume. Tumor and normal tissue %W-O rates of MIBI were calculated on early and late planar (in all patients) (Table 2) and SPECT images (in 23 patients) (Table 1). The same ROIs were used for both early and delayed images to keep the number of pixels unchanged for calculating the %W-O rates. Background correction was applied to all ROIs drawn before calculating %W-O rates. After correction for the physical decay of mean counts in the ROIs drawn on delayed images, the %W-O/hr was calculated for both tumor and normal tissues using the following formula:

$$\% \text{ W-O/hr} = \frac{N(\text{early} - \text{DN}(\text{delayed}))}{N(\text{early}) \times T} \times 100,$$

where N (early) represents the mean counts in the early image, DN (delayed) represents the decay corrected mean counts in the delayed images and T represents the time interval (in hr) between early and delayed images. Because tumor heterogeneity might give rise to different %W-O rates from different parts of the tumor, the tumor and normal tissue %W-O rates from planar images were compared with those from SPECT images (23 patients) to determine whether or not there was any difference between the two- and three-dimensional calculations to avoid possible misleading results that could be obtained from planar images (Table 1).

Technetium-99m-MIBI scans were interpreted by two nuclear medicine physicians who were blinded to the patients' clinical information and immunohistochemistry findings. The tm/bkg ratios and %W-O/hr values were correlated with immunohistochemical findings in all patients.

### Immunohistochemistry

The technique for immunohistochemistry was described in detail elsewhere (8). Briefly, formalin-fixed, paraffin-embedded, 5- $\mu\text{m}$ -thick tissue samples were placed on poly-L-lysine-coated slides (Sigma Chemical Co., St. Louis, MO). The avidin-biotin-peroxidase procedure was used for immunostaining. After deparaffinization and rehydration, the sections were incubated with normal horse serum (Vector Laboratories, Burlingame, CA) for 30 min at 37°C and incubated with primary antibody JSB-1 (Novocastro Laboratory, Cornwall, UK) overnight in a moist chamber at 4°C, at a dilution of 1:20. The tissue sections were incubated with secondary biotinylated horse antimouse antibody and with avidin-biotin-peroxidase complex (Vector). The final reaction product was revealed by exposure to 0.03% diaminobenzidine (Sigma). A negative control was obtained by staining the sample with secondary antibody, and a positive control was obtained by inclusion of a tumor section with known positivity for Pgp. The results of Pgp immunostaining were independently interpreted by two pathologists who had no knowledge of the imaging studies. The tumors were divided into four expression groups with regard to the degree of Pgp positivity on immunostaining (Tables 1 and 2), as follows:

- Group 1: When there was a complete absence of staining for Pgp, tumor samples were scored as “-.”
- Group 2: Scattered positive cells (involvement of <10% of the specimen and weak staining) were scored as “+.”
- Group 3: Focal positivity (focal expression in areas that were <10% of the specimen) was indicated as “f+.”
- Group 4: Diffuse positivity (>10% of the specimen) and weak staining were scored as “++,” and diffuse positivity (>10% of the specimen) and strong staining was scored as “+++.”

**TABLE 2**  
Correlations Between Washout Rates, Tumor-to-background Ratios and P-glycoprotein Expression

Patient no.	tm/bkg	Tumor %W-O*	Normal tissue %W-O*	Pgp	Group	Type	Size (cm)
1	1.3	10	10.5	+++	3	Epid	3.0
2	1.4	9.0	10	++	3	Epid	2.0
3	1.2	9.0	9.5	++	3	SCLC	3.0
4	1.5	6.0	4.0	++	3	SCLC	2.5
5	1.2	16	14	++	3	Epid	2.8
6	2.0	13.5	13	+	2	Epid	3.6
7	2.1	16	16	+	2	SCLC	2.5
8	1.9	12	12.5	+	2	Epid	1.9
9	1.9	12	12	f+	2	Epid	2.0
10	1.9	17	10.5	f+	2	Epid	5.0
11	1.7 nec	16	9.5	f+	2	Epid	6.5
12	1.8	14	12	f+	2	SCLC	2.5
13	2.5	18	14	f+	2	Epid	4.0
14	2.4	13	11	f+	2	Epid	3.0
15	2.4	14	13	f+	2	Epid	3.5
16	2.3	13	10	f+	2	Epid	1.6
17	2.6	11	10	f+	2	Epid	2.8
18	2.3	11	10	f+	2	Epid	2.7
19	2.2	11	13	-	1	Epid	4.0
20	2.8	12	10	-	1	SCLC	3.5
21	2.2	14	12	-	1	SCLC	2.0
22	2.0	11	13	-	1	Epid	4.0
23	2.0	11	12	-	1	Epid	5.0
24	2.5	7.0	8.0	-	1	Epid	2.5
25	2.4	8.0	5.0	-	1	SCLC	1.7
26	2.3	9.0	9.0	-	1	SCLC	2.8
27	2.7	11	12	-	1	SCLC	1.8
28	2.1	15	13	-	1	SCLC	2.6
29	2.3	10	11	-	1	Epid	2.8
30	2.3	12	11	-	1	Epid	2.4
31	2.0	12	11	-	1	SCLC	3.0
32	3.0	13	14	-	1	SCLC	2.0
33	2.0	13	14	-	1	SCLC	3.0
34	2.3	10	11	-	1	SCLC	2.5
35	2.2	10	8.5	-	1	Epid	3.5
36	2.9	10	8.0	-	1	Epid	1.8
37	2.6	13	12	-	1	Epid	3.0
38	2.0	12	10	-	1	SCLC	3.0
39	1.9	11	9.0	-	1	Epid	3.7
40	1.5 nec	13	11	-	1	SCLC	3.0
41	1.9 nec	14	10	-	1	SCLC	3.0
42	1.6 nec	13	12	-	1	Epid	4.0
43	1.9 nec	16	15	-	1	Epid	4.5
44	1.6 nec	12	12.5	-	1	SCLC	2.3
45	1.5 nec	14	12	-	1	SCLC	9.5
46	1.5 nec	13	11	-	1	SCLC	4.5

Epid = epidermoid carcinoma; nec = necrosis detected by radiological modalities or histology.

\*Indicated washout rates were obtained from planar images in all patients.

### Statistical Analysis

The within-subject analyses were performed using the Wilcoxon test to compare tumor and normal tissue %W-O rates with tm/bkg ratios obtained from SPECT and planar studies. Between-subject analyses were performed using the Kruskal-Wallis test among the three groups. The pairwise comparisons were performed with Mann-Whitney U test, with the application of Bonferroni correction when necessary. The significance of correlations between ordinal and numeric data was sought with the Spearman rank correlation test.

### RESULTS

#### Immunohistochemistry

Of the 46 patients, 28 did not have any immunostaining for Pgp, and 5 had strong staining; 10 had only focal expression,

and 3 had scattered positive cells (Table 2). To achieve statistical significance, the patients with focal expression and scattered positivity were evaluated together. The patients were divided into three groups, in relation to the findings on immunohistochemistry, with which the parameters of MIBI imaging were correlated, as follows:

Group 1: Completely negative for Pgp (28 patients) (Fig. 1);

Group 2: Weakly or focally positive for Pgp (+ or f+) (13 patients);

Group 3: Strongly positive for Pgp (5 patients) (Fig. 1).

In our study group, there was no difference in the density of Pgp expression between the patients with SCLC and those with

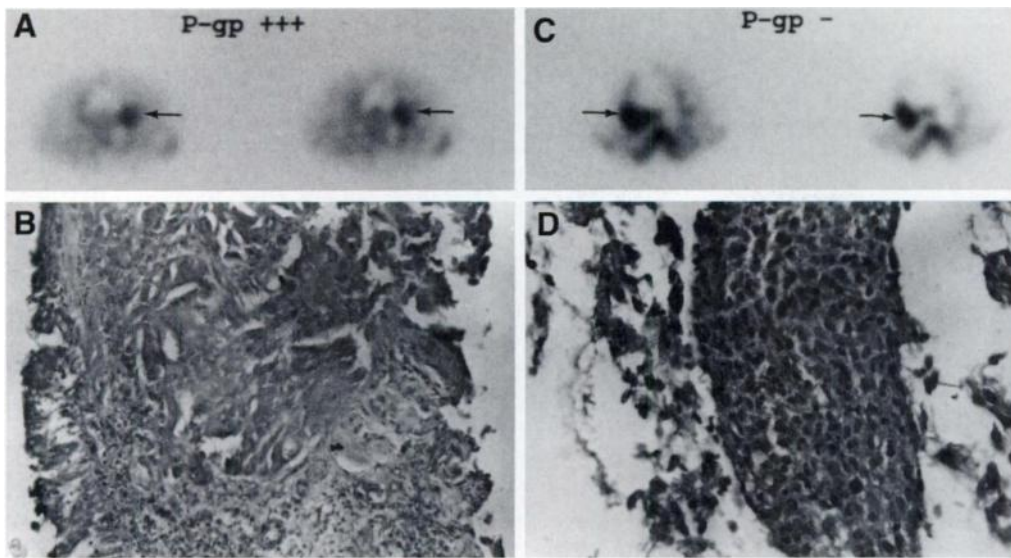


**FIGURE 1.** (A) Technetium-99m-MIBI imaging and bronchoscopic biopsy were performed on a 55-yr-old man with squamous cell carcinoma of the lung. Transverse slices (left, arrows) demonstrate an area of radiotracer uptake in the left perihilar region consistent with the tumor. The tm/bkg ratio was 1.4. (B) Immunohistochemistry reveals strong Pgp expression in the corresponding tumor tissue (lower left). Magnification,  $\times 230$ . (C) Technetium-99m-MIBI imaging and bronchoscopic biopsy were performed on a 48-yr-old woman with squamous cell carcinoma of the lung. Transverse slices (right, arrows) demonstrate an area of intense radiotracer uptake in the right lung fields, consistent with the tumor. The tm/bkg ratio was 2.9. (D) Immunohistochemistry reveals no staining for Pgp (right). Magnification,  $\times 230$ .

epidermoid carcinoma. There were no tumors with accompanying stromal Pgp expression.

#### Percentage Washout Rates Between Tumor and Normal Tissues

Both early and delayed planar and SPECT data were available in 23 patients for calculating tumor and normal tissue %W-O rates (Table 1). Although the numeric values for tumor %W-O rates (mean  $\pm$  s.d. =  $13.9\% \pm 3.4\%$ ) on SPECT data were different from those on planar data ( $11.8 \pm 3.2$ ;  $p = 0.0298$ ; Wilcoxon test) (Table 1), the relative ratios between tumor and normal tissue %W-O rates were not statistically different when derived through SPECT compared to planar imaging ( $p = 0.3604$ ; Wilcoxon test) (Fig. 2). Therefore, we used the %W-O/hr data on planar images in all patients to maintain consistency for the entire patient group (Table 2). When we compared the differences in tumor and normal tissue

%W-O rates among the three groups, none of the groups was statistically different from one another ( $p = 0.3449$ ; Kruskal-Wallis test) (Figs. 2 and 3).

#### Association of Tumor-to-Background Ratios and Percentage Washout Rates with Expression of P-Glycoprotein

The correlations between tm/bkg ratios, %W-O rates and immunohistochemistry findings are summarized in Tables 1 and 2. Because the transport kinetics may differ greatly in necrotic tissues, all tumors with radiographically documented necrotic components were excluded from all three groups and evaluated separately. There was a statistically significant difference in tm/bkg ratios between the three different groups ( $p = 0.0010$ ; Kruskal-Wallis test) (Figs. 1 and 4). Further analysis with the Mann-Whitney U test revealed statistically significant differences in tm/bkg ratios between Groups 1 (mean  $\pm$  s.d. =  $2.32 \pm 0.33$ ) and 3 ( $1.32 \pm 0.13$ ;  $p = 0.0006$ ) (Fig. 4) and between Groups 2 (mean  $\pm$  s.d. =  $2.17 \pm 0.27$ ) and 3 ( $1.32 \pm 0.13$ ;  $p = 0.0015$ ) (Fig. 4). There was no difference between Groups 1 (mean  $\pm$  s.d. =  $2.32 \pm 0.33$ ) and 2 ( $2.17 \pm 0.27$ ;  $p = 0.2659$ ) (Fig. 4).

Because there was no difference between tumor and normal tissue %W-O rates between planar and SPECT data, when correlating %W-O rates with Pgp expression we used only those values obtained from planar images. There was no correlation between the tumor %W-O rates and the level of Pgp

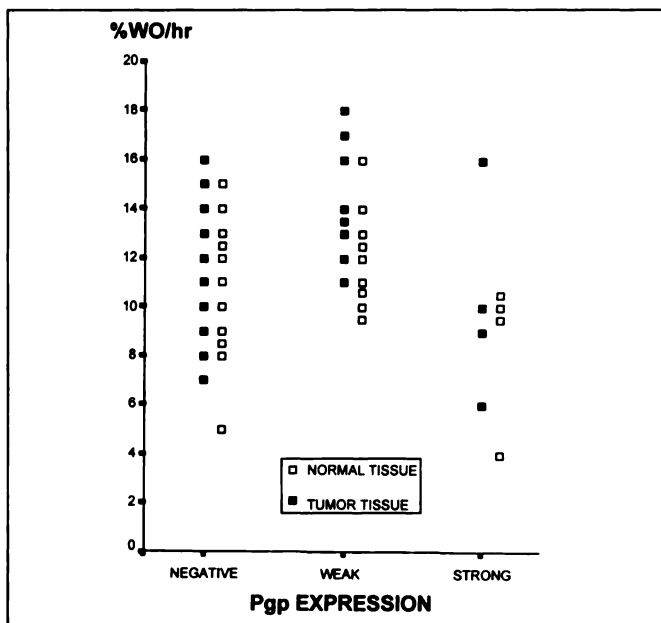


**FIGURE 2.** Tumor (■) %W-O rates of MIBI, as compared with those of normal tissue (□). There was no correlation between tumor %W-O rates and the level of Pgp expression ( $p = 0.414$ ). There was statistically no difference in tumor and normal tissue %W-O rates among the three groups (negative, weak and strong expression) ( $p = 0.3449$ ). (Same numbers that were obtained from different patients were represented as one square in the figure.)

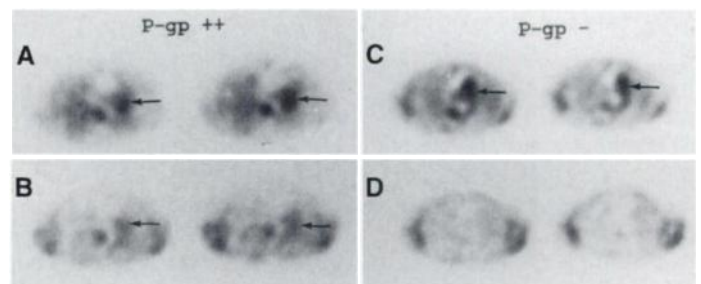


**FIGURE 3.** A 45-yr-old woman with SCLC underwent early (30 min) (A) and delayed (3 hr) (B) MIBI imaging. Immunohistochemistry revealed strong Pgp expression. Transverse slices reveal %W-O of MIBI from the tumor and normal tissues with some residual uptake in the tumor (left, arrows). A 57-yr-old man with SCLC underwent early (30 min) (C) and delayed (3 hr) (D) MIBI imaging. On immunohistochemistry, the tumor was negative for Pgp. Transverse slices reveal %W-O of MIBI from the tumor and normal tissues with no residual uptake in the tumor. No correlation between %W-O rates and Pgp expression was observed.

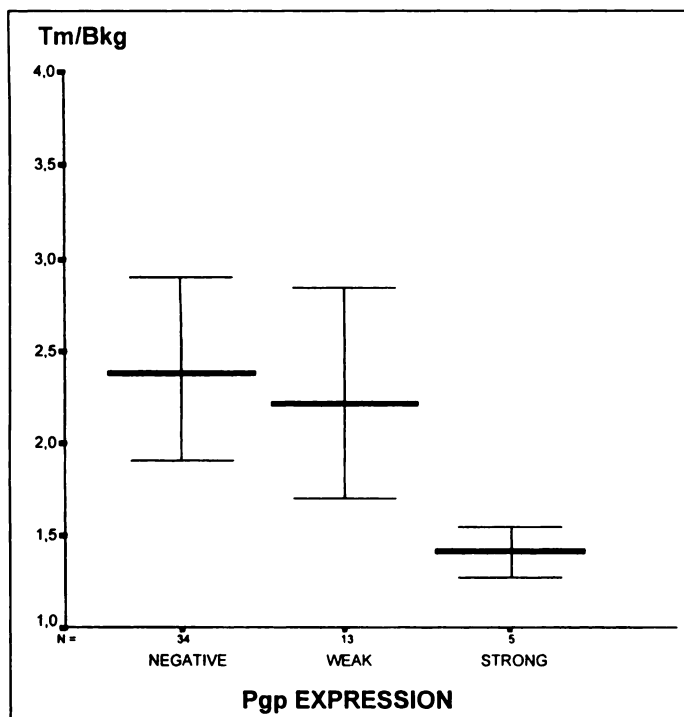


**FIGURE 4.** The correlations between MIBI tm/bkg ratios and the density of Pgp expression in tumor tissues are depicted with mean and s.d. values (represented by solid lines). The values for tm/bkg ratios were significantly lower for those tumors with strong Pgp positivity than those with no detectable or weak expression ( $p = 0.0006$  and  $p = 0.0015$ , respectively).

expression ( $p = 0.414$  and  $r = 0.0137$  by the Spearman rank correlation test) (Fig. 2).

The sizes of the tumors ranged from 1.6 to 5.0 cm (mean  $\pm$  s.d. =  $2.87 \pm 0.83$ ), excluding those with necrosis. There was no correlation between tm/bkg ratios and the size of the tumors ( $p = 0.278$  and  $r = 0.1805$ ; Spearman rank correlation test) when those tumors with necrosis were excluded. Tumor-to-background ratios for epidermoid tumors were not different from those for SCLC when the tumors with necrosis and strong Pgp positivity were excluded (mean  $\pm$  s.d. =  $2.25 \pm 0.28$  and  $2.28 \pm 0.36$ , respectively;  $p = 0.9260$ ; Mann-Whitney U test).

#### Tumors with Necrosis

There was necrosis in eight tumors detected by CT or chest radiograph or histology (Table 2). There was a statistically significant difference between the tm/bkg ratios of tumors with necrosis and those with no necrosis, excluding those with strong Pgp positivity [median = 1.6 (range = 1.5–1.9) compared to 2.3 (1.8–3.0); mean  $\pm$  s.d. =  $1.65 \pm 0.17$  compared to  $2.27 \pm 0.31$  ( $p < 0.0001$ )]. Although this difference was visually conceivable on qualitative evaluation in six tumors, in two, there was no discernible difference on images.

Washout rates of tumors with necrotic component were different from those with no necrosis [median = 13.5 (range = 12–16) compared to 12 (6–18) ( $p = 0.0173$ ; Mann-Whitney U test)].

The sizes of the tumors with necrosis ranged from 3 to 9.5 cm (mean  $\pm$  s.d. =  $4.66 \pm 2.34$ ). There was no statistical correlation between tm/bkg ratios and size of the tumors within this group of patients ( $p = 0.475$  and  $r = 0.1375$  by the Spearman rank correlation test).

#### DISCUSSION

Accurate characterization of Pgp with a noninvasive and practical technique is a topic of ongoing interest (9–12). Most

of the studies regarding the expression of *MDR1* gene have used bulk techniques such as Northern/Western or dot blotting and RNase protection for the detection of Pgp or its messenger RNA. However, the frequently observed contamination with nontumor cells, as well as the heterogeneity within the tumor cell population, constitutes the major disadvantage of such techniques (13–15). Some studies also analyzed the gene expression by immunocytochemistry. Although these in situ methods are more subjective in interpretation than are bulk methods, they provide specific information on the MDR expression levels in individual cells and the morphology and the localization of the MDR-expressing cells. Recently, as a functional imaging agent, MIBI has been reported to be a transport substrate recognized by Pgp, providing a means to noninvasively characterize Pgp expression in tumors in vivo (6,7). However, despite the extensive in vitro work performed thus far, its clinical relevance has yet to be defined (6,7,16).

In full agreement with previous in vitro work and our prior clinical study, the current data revealed that the tm/bkg ratios obtained from MIBI imaging were inversely proportional with the density of Pgp (Figs. 1 and 4) (6,7,16,17). Also, in line with our previous findings, the present data suggested that focal or scattered expression of Pgp has little impact on the MIBI uptake (17). On the basis of these findings, one could deduce that on clinical grounds, a threshold level should be reached for Pgp mechanism to be therapeutically significant.

P-glycoprotein functions as an ATP-dependent efflux pump. Although the manner in which the energy of ATP is harnessed to reduce drug accumulation in cells expressing MDR genes is unknown, it is postulated that the reduced substrate accumulation is the consequence of a decrease in steady-state drug accumulation and an increase in efflux of the substrates. In the literature, controversies and contradictions exist regarding the relationship between these two features, justifying further studies to determine the extent of contribution of each component. Assuming that Pgp acts as a drug transporter mediating drug efflux, one would expect a close connection between Pgp expression and enhanced %W-O of the substrates from the tumors. Conversely, some investigators were unable to detect an active efflux mechanism associated with the considerable reduction in substrate accumulation in some resistant cell lines with increased Pgp expression (4,18,19). Likewise, in this preliminary data, although we had only five patients with strong Pgp positivity, we did not observe any correlation between tumor %W-O rates of MIBI and the density of Pgp (Fig. 4). As observed in our data, some hypotheses suggest that Pgp acts as a “flipase,” directly flipping proteinated drug from the inner to the outer leaflet of the lipid bilayer without allowing the drug to accumulate at high proportions within the cell (20). In this context, %W-O rates are not supposed to be affected dramatically as soon as the drug loses contact with the membrane after reaching the cytoplasm. Also, like colchicine, the uptake of which was found to remain linear over 2 hr with no demonstrable efflux due to tight binding to tubulin in the cytoplasm (4), MIBI being sequestered into the mitochondria by negative membrane potentials could escape the outward transport component of Pgp pump once it reaches the mitochondria. Alternatively, Pgp efflux pump could be a rapidly functioning mechanism that reaches an equilibrium within a short period while maintaining a stable level of extrusion, at which the %W-O rate from the tumor approximates that of normal tissue at 30 min and beyond. On the other hand, the heterogeneity of Pgp expression might account for different and inconsistent %W-O rates of MIBI through varying Pgp function capacities and %W-O rates. Here, it is also noteworthy to emphasize the fact

that our results could be due to the detection limit of the imaging procedures to detect subtle variations in transport kinetics.

The transport of any radiotracer is also governed by biological properties of the diffusing molecules. Similarly, in this study, the tumors with necrotic components had significantly lower  $tm/bkg$  ratios than those with no necrosis excluding those with strong Pgp positivity ( $p < 0.0001$ ), probably because of poor vascularization. Additionally, they had faster %W-O rates as compared with the rest of the group ( $p = 0.0173$ ), most likely due to unfavorable pharmacokinetics and inadequate number of viable mitochondria for MIBI to be sequestered into. Therefore, extreme caution should be exercised when the scans of those patients with necrotic tumors are interpreted to avoid false-positive results.

Despite the fact that SCLC is associated with progressive refractoriness to chemotherapy, in our study, there was not any difference in Pgp expression between the patients with SCLC and those with epidermoid cancer ( $p = 0.926$ ). Nonetheless, this should not be a surprising finding because previous studies have shown frequent occurrence of non-Pgp-mediated MDR in SCLC (21,22). Moreover, various investigations revealed only low levels of *MDR1* expression in patients with lung cancer, including both SCLC and non-SCLC (20,23,24). P-glycoprotein belongs to a superfamily of ATP-binding cassette transporters, and, recently, a new member of this family called MDR-associated protein (MRP) has been cloned from human lung cancer cell lines. Therefore, expression of the MRP gene may be a significant factor determining response of lung cancer to therapy (24). In line with these previous observations, in our current study, only 11% of the specimens showed strong and 28% focal or scattered Pgp positivity. Cells of this type of resistance do not have accumulation defects, so the lack of observable %W-O alterations in our patients might corroborate the hypothesis that the MRP gene is more relevant than the MDR gene in lung cancer (24–27).

### Study Limitations

Immunocytochemistry is subjective in interpretation; however, as we did in this study, evaluation of immunostaining by the same experienced pathologist may provide better comparisons, although the quantity of antigen could not be determined. The intention of this study was not to quantitate the antigenic sites but providing estimates of antigen expression in mass units using quantitative autoradiography would certainly clarify many aspects of Pgp expression. However, antigenic heterogeneity might still influence the accuracy of quantitative autoradiography results (28,29).

Although sequential imaging at multiple time points should be performed to accurately calculate %W-O rates, due to time constraints and inconvenience, we obtained images at only two time points. Because, at 30 min, some efflux might have already started to take place, one might think that taking 30 min as the reference time for initial tumor uptake could easily lead to erroneous results. However, according to the unpublished data we obtained on two patients (not included in this study) with strong Pgp positivity, the percentages of maximum tumor uptake of MIBI at 30 min were 85% and 92%, respectively. Although these data are preliminary, it suggests that, at 30 min, there should still be a considerable amount of radioactive material left in the tumor that could allow one to determine %W-O rates. The other shortcoming of this study was the calculation of %W-O rates using only two time points, which could introduce important errors. However, again in our unpublished data, the clearance of MIBI was quadratic, but it could be

fit into a linear curve with a maximum error of 3.87%, which rendered our extrapolation much less erroneous.

Lung tumors, especially SCLCs, are the least conducive to the evaluation of Pgp distribution because most specimens are obtained through bronchoscopic biopsy, which might not represent the entire tumor characteristics. In this study, however, our initial step before calculating %W-O rates was to verify the relationship between the levels of Pgp with  $tm/bkg$  ratios of MIBI imaging, which represent the entire tumor. Therefore, based on our confirmation of an inverse relationship between  $tm/bkg$  ratios and the level of Pgp expression, we believe that the samples we studied were good representatives of the tumor characteristics.

### CONCLUSION

Although we did not have a large number of patients with strong Pgp positivity, our attempt to determine the association of MIBI %W-O rates with Pgp expression failed to find any correlation between these two germane concepts in this patient group. Nonetheless, this clinical study supported the results of our first study by finding a strong agreement between the occurrence of increased Pgp expression and decreased cellular MIBI accumulation (17). In light of this consistent finding, MIBI imaging could be used as a noninvasive test in guiding treatment when Pgp is pertinent. But, it should also be borne in mind that tumors with necrosis could be sources of potential confusion. We believe that the accuracy of our findings should be reproduced by further studies with extended number of patients.

### REFERENCES

1. Endicott JA, Ling V. The biochemistry of P-glycoprotein-mediated multidrug resistance. *Annu Rev Biochem* 1989;58:137–171.
2. Fojo AT, Ueda K, Slamon DJ, Poplack DG, Gottesman MM, Pastan I. Expression of a multidrug-resistance gene in human tumors and tissues. *Proc Natl Acad Sci USA* 1987;84:265–269.
3. Biedler J. Genetic aspects of multidrug resistance. *Cancer* 1992;70:1799–1809.
4. Nielsen D, Skovsgaard T. P-glycoprotein as multidrug transporter: a critical review of current multidrug resistant cell lines. *Biochim Biophys Acta* 1992;1139:169–183.
5. Chiu ML, Kronauge JF, Piwnica-Worms D. Effect of mitochondrial and plasma membrane potentials on accumulation of hexakis (2-methoxyisobutylisocyanide) technetium(I) in cultured mouse fibroblasts. *J Nucl Med* 1990;31:1646–1653.
6. Piwnica-Worms D, Chiu ML, Budding M, Kronauge JF, Kramer RA, Croop JM. Functional imaging of multidrug-resistant Pgp with an organotechnetium complex. *Cancer Res* 1993;53:977–984.
7. Rao VV, Chiu ML, Kronauge JF, Piwnica-Worms D. Expression of recombinant human multidrug resistance P-glycoprotein in insect cells confers decreased accumulation of technetium-99m-sestamibi. *J Nucl Med* 1994;35:510–515.
8. Baldini N, Scotlandi K, Barbanti-Brodano G, et al. Expression of P-glycoprotein in high-grade osteosarcomas in relation to clinical outcome. *N Engl J Med* 1995;333:1380–1385.
9. Ross DD, Thompson BW, Ordonez JV, Joneckis CC. Improvement of flow-cytometric detection of multidrug-resistant cells by cell-volume normalization of intracellular daunorubicin content. *Cytometry* 1989;10:185–191.
10. Chan H, Thoner P, Haddad G, Ling V. Immunohistochemical detection of P-glycoprotein: prognostic correlation in soft tissue sarcoma of childhood. *J Clin Oncol* 1990;8:689–704.
11. Kessel D, Beck WT, Kukuruga D, Schulz V. Characterization of multidrug resistance by fluorescent dyes. *Cancer Res* 1991;51:4665–4670.
12. Noonan KE, Beck WT, Holzmayer TA, et al. Quantitative analysis of *MDR1* (multidrug resistance) gene expression in human tumors by polymerase chain reaction. *Proc Natl Acad Sci USA* 1990;87:7160–7164.
13. Epstein J, Xiao H, Oba BK. P-glycoprotein expression in plasma cell myeloma is associated with resistance to VAD. *Blood* 1989;74:913–917.
14. Mae J-P, Zittoun R, Sikic BI. Multidrug resistance (*mdr1*) gene expression in adult acute leukemias: correlation with treatment outcome and in vitro drug sensitivity. *Blood* 1991;78:586–592.
15. Nooter K, Herweijer H. Multidrug resistance (*mdr*) genes in human cancer. *Br J Cancer* 1991;63:663–669.
16. Duran Cordobes M, Starzes A, Delmon-Moingeon L, et al. Technetium-99m uptake by human benign and malignant breast tumor cells: correlation with *mdr* gene expression. *J Nucl Med* 1996;37:286–289.
17. Kostakoglu L, Elahi N, Kiratli P, et al. Clinical validation of influence P-glycoprotein on the uptake of technetium-99m-sestamibi in patients with malignant tumors. *J Nucl Med* 1997;1003–1008.
18. Ramu A, Pollard HB, Rosario LM. Doxorubicin resistance in P388 leukemia-evidence for reduced drug influx. *Int J Cancer* 1989;44:539–547.

19. Deffie AM, Alam T, Seneviratne C, et al. Multifactorial resistance to Adriamycin: relationship of DNA repair, glutathione transferase activity, drug efflux and P-glycoprotein in cloned cell lines of Adriamycin-sensitive and resistant P388 leukemia. *Cancer Res* 1988;48:3595-3602.
20. Chin K-V, Pastan I, Gottesman MM. Function and regulation of the human multidrug resistance gene. *Adv Cancer Res* 1993;60:157-180.
21. Lai SL, Goldstein LJ, Gottesman MM, et al. *MDR1* gene expression in lung cancer. *J Natl Cancer Inst* 1989;81:1144-1150.
22. Binaschi M, Supino R, Gambetta RA, et al. *MRP* gene overexpression in human doxorubicin-resistant SCLC cell line: alterations in cellular pharmacokinetics and in pattern of cross-resistance. *Int J Cancer* 1995;62:84-89.
23. Goldstein LJ, Gaski H, Fojo A, et al. Expression of a multidrug resistance gene in human cancers. *J Natl Cancer Inst* 1989;81:116-124.
24. Eijddems, De Haas M, Coco-Martin JM, et al. Mechanisms of MRP over-expression in four human lung-cancer cell lines and analysis of the MRP amplicon. *Int J Cancer* 1995;60:676-684.
25. Thomas GA, Barrand MA, Steward S, Rabbitts PH, Williams ED, Twentyman PR. Expression of the multidrug resistance-associated protein (MRP) gene in human lung tumors and normal tissue as determined by in situ hybridisation. *Eur J Cancer* 1994;30A:1705-1709.
26. Giaccone G, van Ark Otte GJ, et al. MRP is frequently expressed in human lung cancer cell lines in non-small-cell lung cancer and in normal lungs. *Int J Cancer* 1996;66:760-767.
27. Sugawara I, Yamada H, Nakamura H, et al. Preferential expression of the multidrug resistance-associated protein (MRP) in adenocarcinoma of the lung. *Int J Cancer* 1995;64:322-325.
28. Del Vecchio S, Stoppelli P, Carriero MV, et al. Human urokinase receptor concentration in malignant and benign breast tumors by *in vitro* quantitative autoradiography: comparison with urokinase levels. *Cancer Res* 1993;53:3198-3206.
29. Li PY, Del Vecchio S, Fonti R, et al. Local concentration of folate binding protein GP38 in sections of human ovarian carcinoma by *in vitro* quantitative autoradiography. *J Nucl Med* 1996;37:665-672.

## Fluorine-18-Fluorodeoxyglucose Uptake in Rheumatoid Arthritis-Associated Lung Disease in a Patient with Thyroid Cancer

Siema M.B. Bakheet and John Powe

Department of Radiology, King Faisal Specialist Hospital and Research Center, Riyadh, Saudi Arabia

An <sup>18</sup>F-fluorodeoxyglucose (FDG) whole-body PET scan was performed on a thyroid cancer patient with long-standing rheumatoid arthritis who presented with pulmonary nodules. A recent diagnostic radioiodine whole-body scan was negative. However, the <sup>18</sup>F-FDG scan demonstrated intense uptake in the chest lesions as well as in several joints affected by rheumatoid arthritis. Fine-needle aspiration of a pulmonary nodule revealed inflammatory reaction and absence of malignant cells, fungus and tuberculous infection. A repeat chest CT scan after 7 mo of steroid therapy showed a marked decrease in the size and number of nodules. In thyroid cancer patients, <sup>18</sup>F-FDG uptake in the lung may not necessarily represent pulmonary metastases. This case illustrates a benign, unrelated pathology namely, rheumatoid arthritis-associated lung disease.

**Key Words:** fluorine-18-fluorodeoxyglucose; PET; rheumatoid arthritis; thyroid cancer; false-positive results

**J Nucl Med** 1998; 39:234-236

**F**luorine-18-fluorodeoxyglucose (FDG) PET imaging has a proven role in the assessment of patients with cancer (1). It has been useful in detecting suspected or proven recurrence and/or metastases of differentiated thyroid cancer (2). Since differentiated thyroid cancer is not uncommon, coexistent unrelated pathology in thyroid cancer patients may represent a diagnostic problem. We report on a thyroid cancer patient who presented with chest lesions with <sup>18</sup>F-FDG uptake due to rheumatoid arthritis-associated lung disease.

### CASE REPORT

A 57-yr-old woman with long-standing rheumatoid arthritis and a history of papillary thyroid cancer presented with pulmonary nodules on a chest radiograph. The patient had a 12-yr history of rheumatoid arthritis with secondary Sjogren's syndrome. Two years earlier, she had a right, followed by complete, thyroidectomy

for a large cold nodule in the right lower lobe. The histology showed a follicular variant of papillary thyroid cancer confined to the thyroid gland. A laboratory workup showed an erythrocyte sedimentation rate of 69 mm/hr, a rheumatoid factor of 43 IU/ml (normal range 0-19) and positive for antinuclear antibodies (speckled) 1:640 with a diagnostic 555 MBq (15 mCi).

A <sup>123</sup>I whole-body scan showed 18% neck uptake, for which the patient received 4440 MBq (120 mCi) <sup>131</sup>I treatment. An initial chest radiograph revealed several pulmonary nodules that were subsequently shown on a chest CT scan (Fig. 1A). One year later, a follow-up chest CT scan showed an increase in the size and number of pulmonary nodules as well as some cavitation (Fig. 1B and 1C). A concurrent radioiodine diagnostic scan was negative (thyroid-stimulating hormone 170 mU/liter; thyroglobulin 2.6 μ/liter). Sputum samples were consistently negative for tuberculosis and malignancy. Several months later, a whole-body <sup>18</sup>F-FDG PET scan 1 hr postinjection of 370 MBq (10 mCi) showed corresponding uptake in all lung nodules as well as in several joints (Fig. 2). A CT scan-guided fine-needle aspiration of the lesion in the basal part of the right lung revealed giant inflammatory cells and the absence of malignant cells, fungus and tuberculous infection.

The patient was given 40 mg prednisone orally daily for 5 wk, with a gradual tapering of the dose to 10 mg daily over a period of 8 wk. A chest CT scan 7 mo later showed considerable resolution of the chest lesions (Fig. 1D). The patient had no clinical, biochemical or scintigraphic evidence of persistent or recurrent thyroid cancer up to 2.5 yr after radioiodine treatment and was maintained on thyroxine 150 μg and prednisone 10 mg daily.

### DISCUSSION

We present rheumatoid arthritis-associated lung disease causing FDG uptake in a patient with papillary thyroid cancer. The presence of pulmonary nodules on a routine chest radiograph suggested pulmonary metastases. The absence of radioiodine uptake in the chest lesions together with the undetectable thyroglobulin levels argued against it.

Fluorine-18-FDG uptake was noted in all nodules seen on the CT scan as well as in the inflamed joints. The scan appearance

Received Aug. 29, 1996; revision accepted Apr. 14, 1997.

For correspondence or reprints contact: Siema M.B. Bakheet, MD, Nuclear Medicine, Department of Radiology (MBC #28), King Faisal Specialist Hospital and Research Center, P.O. Box 3354, Riyadh 11211, Kingdom of Saudi Arabia.